

EXPERIMENTAL INVESTIGATIONS OF FLOW THROUGH WIDE ANGLE CONICAL DIFFUSERS WITH UNIFORM FLOW AND SWIRL TYPE VELOCITY DISTORTIONS AT INLET

by

Arumugam HEMALATHA* and **Nainangkuppam Venkatesan MAHALAKSHMI**

Department of Mechanical Engineering, College of Engineering Guindy, Anna University,
Chennai, Tamil Nadu, India

Original scientific paper
<https://doi.org/10.2298/TSCI170817223H>

Swirl is a tangential velocity component of the fluid flow and is often present in the conical diffuser as a result of rotating machinery in the upstream section. The present experimental work is dedicated to study the effect of moderate swirl on wide angle conical diffuser performance and flow development. The experiments were performed in a low-speed open circuit wind tunnel. There are two different diffusers having a cone angle of 14° (with an area ratio 3.0) and 20° (with an area ratio 4.2) were selected for this investigation. The flow parameters have been measured using DANTEC DYNAMICS make constant temperature hot-wire anemometer (CTA). The results showed that the moderate swirl can significantly improve the stalled diffuser (20° cone angle) performance; however, it has a little effect on the diffuser (14° cone angle) having incipient turbulent boundary layer separation. It was confirmed that the introduction of moderate swirl reduces the chances of flow separation in wide angle conical diffusers.

Key words: conical diffuser, displacement thickness, hotwire anemometer, swirl, tangential velocity

Introduction

Diffusers are widely used in fans, pumps, turbines, compressors, and many other fluid machines. In its simplest form, a diffuser is a diverging passage in the flow direction, in which the kinetic energy is converted to pressure energy by decelerating the flow. This energy conversion process of the diffuser decides the fluid machine performance. Over the decades, a large number of research works have been pursued to understand the mechanism which governs the performance of diffuser with the uniform flow and with inlet velocity distortions. Swirling inlet flow is an important practical case of inlet flow distortions. Various researchers have attempted to study the effect of swirl on conical diffuser performance.

Mc Donald and Fox [1] conducted an experiment in a transparent conical diffuser using water as the flow medium. They concluded that the pressure recovery and effectiveness are independent of the inlet Reynolds number if it is greater than 75000. Okwuobi and Azad [2] conducted experiments to study the structure of turbulence in a conical diffuser with fully developed flow at entry. They reported that the rate of turbulent energy production reaches the maximum value at the edge of the wall layer extending to the point of maximum u' fluctuation.

* Corresponding author, e-mail: hemathanga27@gmail.com

Klein [3] reviewed thirty publication results in the subject of the effect of inlet conditions on the performance of conical diffuser flow. From the review results, he presented the optimum diffuser geometries for non-dimensional diffuser length. Azad [4] made an extensive research work in turbulent flow through an 8° cone angle diffuser. The measurement of fourth-order moments of turbulence fluctuations showed that the turbulent flow is symmetrical for all mean values in a conical diffuser. Mahalakshmi *et al.* [5] studied experimentally the effect of wake type velocity distortions at the inlet of conical diffusers. They observed that the wake at inlet greatly affects the diffuser performance.

Van Dewoestine *et al.* [6] conducted experiments to study the effect of swirling inlet flow on the performance of conical diffusers. The results showed that the swirling inlet flow increases the performance of optimum diffuser compared to the uniform flow at the inlet. Senoo *et al.* [7] and Okhio *et al.* [8] suggest from their experimental study in a conical diffuser that the moderate swirl will delay the flow separation and increase the pressure recovery. Clausen *et al.* [9] made detailed measurements of turbulence quantities for a 20° conical diffuser having swirl flow.

A considerable amount of theoretical investigations has been done on conical diffusers. Lai *et al.* [10] investigated the effect of the adverse pressure gradient in conical diffuser using $k-\varepsilon$ model. Jiang *et al.* [11] adopted DLR $k-\varepsilon$ model to study the internal turbulent flow in a conical diffuser. Armfield and Fletcher [12] studied the swirl effect in a conical diffuser using $k-\varepsilon$ model and Reynolds stress model. Chou and Fletcher [13] concluded that their Algebraic Reynolds model predicts the swirl flow better than the $k-\varepsilon$ model. Okhio *et al.* [14] selected Prantl mixing length model to calculate the mean velocities in a wide-angle conical diffuser. Recently, From *et al.* [15] modeled turbulent swirling flow in a conical diffuser using the Explicit Algebraic Reynolds stress model.

The present work is mainly concerned with the experimental study of the flow and boundary layer development in conical diffusers with the steady, uniform flow and moderate swirl type distorted flow at the entry of the diffuser. The experiments were conducted in a subsonic wind tunnel using a constant temperature hot-wire anemometer (CTA) measurement system.

Experimental set-up and measurements

The experiments were conducted in a blower driven, low-speed wind tunnel set-up. The line sketch of the wind tunnel is shown in fig. 1. The wind tunnel facility consists of a blower, settling chamber and a bell-mouthed nozzle. The blower is driven by an 11 kW motor running at a constant speed of 2500 rpm. The dimensions of the settling chamber are $1 \times 1 \times 2$ m. The four-layer No. 80 metallic screens are placed in the settling chamber. These fine meshes

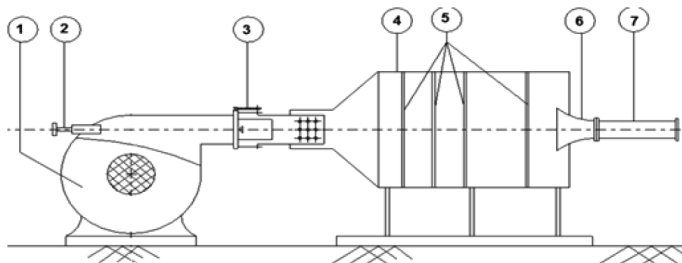


Figure 1. Schematic diagram of wind tunnel facility; 1 – blower, 2 – bypass control, 3 – throttle control, 4 – settling chamber, 5 – screens, 6 – bell-mouth nozzle, and 7 – pipe

reduce the turbulence level of the incoming air. The flow velocity and the mass flow rate at the exit of the wind tunnel could be altered by throttle control. A pipe of 100 mm internal diameter and a length of 600 mm was fitted at the exit of the wind tunnel to achieve a fully developed flow.

The present measurements were carried out using a DAN-

TEC DYNAMICS make constant temperature hot-wire anemometer (CTA). The CTA works on the principle of convective heat transfer to the flow medium from an electrically heated thin wire. Flow parameters have been measured using an X-array probe of type 55P61. An over-heating ratio (relating factor to cold resistors to the warm resistors at the Wheatstone bridge operating conditions) is set 0.8 for the current measurements. The X-array probe was calibrated using an eight-hole pitot-static tube with digital manometer read out.

The velocity calibration is carried out for the known velocities of range from 10-35 m/s. Calibration demonstrates a relationship between the probe corrected voltages (E_{1corr} , E_{2corr}) and the flow velocities (U_{1cal} , U_{2cal}) using a fourth order polynomial fit [16]. National Instruments analog-to-digital converter (A/D board NI6040E (PCI – M10 – 16E – 4)) was used for data acquisition. Figure 2 shows the experimental set-up.

Flow parameters were measured seven stations across the axis of the diffuser. The measurement stations were designated as A, B, C, D, E, F, and G. The distance between the measuring stations from the inlet of the diffuser is given in tab. 1 and represented in fig. 3. The reference station for flow measurements is located in the inlet pipe at $X = -30$ mm [9]. Mean flow parameters of the reference station, air temperature of 29.5 °C, are listed in tab. 2.



Figure.2. Experimental set-up

Table 1. Measuring stations

Stations	A	B	C	D	E	F	G
X [mm]	30	60	90	120	150	180	210
X/L	0.1	0.2	0.3	0.4	0.5	0.6	0.7

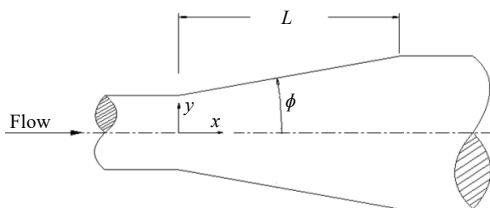


Figure 3. Location of measuring sections

Table 2. Mean flow parameters at reference station

Reynolds number, ($= UD/\nu$), [-]	225000
Mean velocity, U [ms^{-1}]	35
Kinematic viscosity, ν [m^2s^{-1}]	$1.59 \cdot 10^{-5}$
Density, ρ [kgm^{-3}]	1.166

Conical diffuser

Conical diffusers having a half cone angle, ϕ , of 7° (area ratio 3.0) and 10° (area ratio 4.2) have been selected for the present investigations. These half cone angles and area ratios are sufficient to cause separated flow without any inlet velocity distortions. The 14° cone angle diffuser is machined from a solid steel cylinder, which gives a smooth divergence section. The geometric details of the 14° conical diffuser are shown in fig. 4(a). To reduce the surface roughness, the 20° cone angle diffuser is made of perspex sheet. The photographic view of the test diffusers is shown in fig. 4(b). The conical diffuser inlet section is connected with a pipe of 100 mm internal diameter and a length of 300 mm to place the swirl generator. The conical diffuser exit is connected with a tailpipe of length 300 mm.

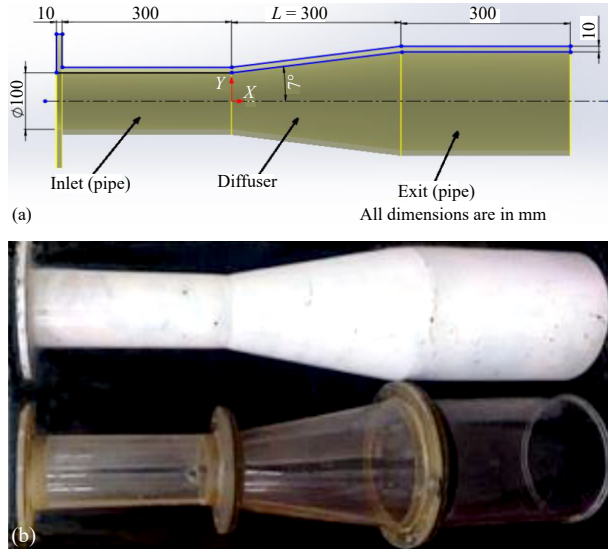


Figure 4. (a) Schematic illustration of conical diffuser (14°) and (b) photographic view of the conical diffusers

For the present case, the swirl generator with $\beta = 25^\circ$, generates a moderate swirl of $S = 0.18$. The swirl generator was machined from a solid aluminum cylinder block of diameter 100 mm.

Geometry and fabrication of swirl generator

To obtain a swirling flow, the four channel swirl generator was designed and fabricated [17]. Figure 5(a) shows the photographic view of the swirl generator selected for the present investigation to generate a swirl type velocity distortion at the inlet of the diffuser. The detailed dimensions of the swirl generator used in the present experiment are shown in fig. 5(b). The swirl number for an annular swirl generator can be calculated from:

$$S = \frac{2}{3} \left(\frac{1 - \alpha^3}{1 - \alpha^2} \right) \tan \beta \quad (1)$$

where α is the hub ratio and β is the channel angle.

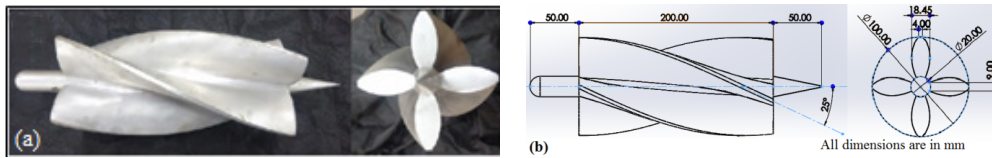


Figure 5. (a) Photographic view of swirl generator and (b) geometry of the swirl generator

Measurement uncertainties

DANTEC DYNAMICS constant temperature hot wire anemometer (CTA) follows an ISO uncertainty model to calculate the uncertainty of the measurements [16]. This ISO model calculates the total uncertainty $[G(tot)]$ as a combination of relative uncertainty of every individual output variable, $y_i = f(x_i)$, at a given confidence level.

The total uncertainty is defined:

$$G(tot) = 2\sqrt{\sum [g(y_i)]^2} \quad (2)$$

Here, the relative standard uncertainty $g(y_i)$ is a function of the standard deviation of the input variables:

$$g(y_i) = \frac{1}{y_i} \left(\frac{\partial y_i}{\partial x_i} \right) \left(\frac{\Delta x_i}{k_i} \right) \quad (3)$$

where $(\partial y_i / \partial x_i)$ is the sensitivity factor and k_i is the coverage factor.

The uncertainty of measured velocity with hot-wire anemometer mainly depends on the instrument, calibration equipment, and experimental conditions. The uncertainties related to experimental conditions are probe positioning, temperature variations, and humidity changes.

- *Anemometer uncertainty.* Drift, noise, repeatability and frequency response are the main causes for this uncertainty. As low drift, low noise and good repeatability are the characteristics of the commercial anemometer, their contribution to the total uncertainty is negligible compared to other error sources.
- *Uncertainty due to calibration equipment.* The selection of calibration equipment constitutes the major source of uncertainty. Here, a pitot-static tube with micro-manometer was used for calibration. The relative standard uncertainty is stated to be $\pm 2\%$.
- *Linearization (conversion) related uncertainty.* The linearisation uncertainty is due to the curve fitting errors. Here, the curve fitting is taken care of Streamware software and specified as the 0.5% of the measured velocity.
- *Uncertainty related to data acquisition.* The A/D board resolution uncertainty mainly depends on the A/D board input voltage range ($E_{AD} = 0-10$ V), its resolution in bits ($n = 12$ bit) and the sensitivity factor (slope of the inversion calibration curve [$U = F(E)$]), which is estimated to be $(\partial U / \partial E) = 37.33$ (m/s)/V.
- *Uncertainty due to probe positioning.* The probe is positioned with an uncertainty of 1° (θ).
- *Uncertainty due to temperature variations.* Temperature variations from calibration to experiment or during experiment introduce this error. Temperature variation changes the sensor over temperature ($T_w - T_0$). This uncertainty is expressed:

$$\frac{1}{\sqrt{3}} \left(\frac{1}{U} \right) \left(\frac{\Delta T}{T_w - T_0} \right) \left(\frac{A}{B} U^{-0.5} + 1 \right)^{0.5} \quad (4)$$

where $A = 2.3152$, $B = 0.853$ (calculated from the calibration velocity fit using the power law scheme). Measured sensor over temperature ($T_w - T_0$) is 231°C . The ΔT is specified as 1°C .

- *Uncertainty due to humidity.* Changes in humidity affect the vapor pressure of the air and thus the heat transfer. The influence of heat transfer in standard uncertainty is very small, $\partial U / \partial P_{wv} \approx 0.01U$ per 1 kPa change in water vapor pressure P_{wv} .

The uncertainties obtained with a single-sensor hot-wire probe is summarized in tab. 3.

Results and discussion

Performance

Generally, the diffuser performance is stated by a pressure recovery coefficient, C_p . It indicates the diffuser ability of the diffuser to convert kinetic energy into pressure energy. The pressure recovery coefficient can be calculated [9, 18]:

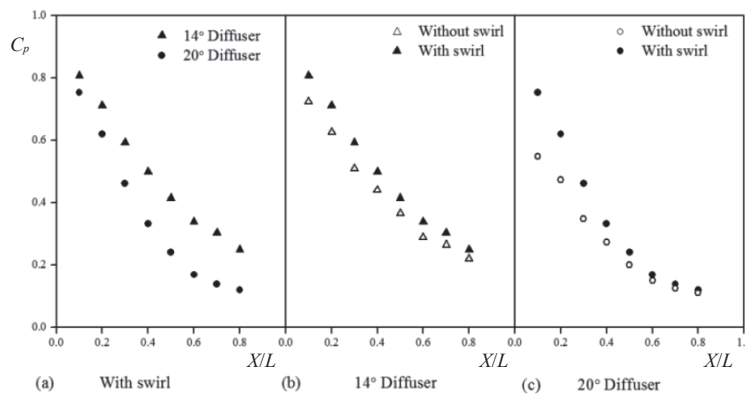
$$C_p = \frac{P_x - P_a}{q_x} \quad (5)$$

where P_x is the average static pressure at each station, P_a – the atmospheric pressure, and q_x – the dynamic head of the respective station. The static pressure at each station is measured using eight-hole pitot-static tube with digital manometer read out, by traversing probe at an interval of 4 mm. The measurements of static pressure are made relative to the atmospheric pressure exposing one of the leads of the manometer to the atmosphere.

Figure 6 illustrates the performance of the conical diffusers with uniform velocity and swirl at the inlet. It can be noticed that there is a marginal increase in pressure recovery in the

Table 3. Uncertainty of hot-wire measurements

Source of uncertainty	Input Δi	Input value	Output $(1/U)\Delta y_i$	Output value	Coverage factor $[k_i]$	Standard uncertainty, $g(y_i)$
Calibrator, g_{cal} (Pitot tube)		$\pm 2\%$	$2\left(\frac{1}{100}\right)(Accuracy\%)$	0.04	2	0.02
Linearization, g_{fit}		0.5%	$2\left(\frac{1}{100}\right)(error\%)$	0.01	2	0.005
A/D board resolution, g_{AD}	$\frac{E_{AD}}{n}$	10 V 12 bit	$\left(\frac{1}{U}\right)\left(\frac{E_{AD}}{2^n}\right)\left(\frac{\partial U}{\partial E}\right)$	0.0026	$\sqrt{3}$	0.0015
Probe positioning, g_{θ}	θ	1 °	$1 - \cos\theta$	0.0015	$\sqrt{3}$	≈ 0
Sensor over temperature, g_{temp}	ΔT	1 °C	$\left(\frac{1}{U}\right)\left(\frac{\Delta T}{T_w - T_0}\right)\left(\frac{A}{B}U^{-0.5} + 1\right)^{0.5}$	0.00014	$\sqrt{3}$	0.00008
Humidity, g_H	ΔP_{wv}	0.1 kPa	$\left(\frac{1}{U}\right)\left(\frac{\partial U}{\partial P}\right)\Delta P_{wv}$	0.0001	$\sqrt{3}$	≈ 0
Total uncertainty = $G_{tot} = 2\sqrt{\sum u(y_i)^2} = 0.043 = 4.3\%$						

**Figure 6. Variation of pressure recovery coefficient (C_p) in 14° diffuser and 20° diffuser**

case of flow with swirl when compared to uniform flow for the diffusers. It is also observed from the figures that 50% of pressure recovery takes place within the first 40% length of the diffuser.

Mean velocity profiles

Mean axial velocity

The measured axial velocity and the cross stream distance across the measuring station are non-dimensionalized with the mass averaged velocity, \bar{U} , and with the diffuser radius, $Y(N)$, respectively, at the corresponding station. Figures 7 and 8 illustrate the normalized velocity profiles for 14° and 20° cone angle diffusers, respectively, for the case of uniform flow and swirl flow at the inlet. It is seen that in the uniform flow at the inlet, the flow distortion is only due to the boundary layer development. It was observed from fig. 7 in the case of 14°

cone angle diffuser without swirl flow indicates that the boundary layer thickness is initially 10 % ($Y/Y(N) \approx 0.9$) at $X/L = 0.1$, which has grown to 70% at $X/L = 0.7$. Here, it was confirmed from the velocity profiles of the 14° cone angle diffuser, without any inlet velocity distortion the flow tends to separate from the wall (incipient flow separation).

Further, for the case of 20° cone angle diffuser flow with uniform velocity at the inlet, the flow separation was observed from $X/L = 0.5$ onwards. The hot-wire probes do not have the directional sensitivity; it cannot show the negative values (flow separation) of the velocity readings. Hence, the separated (reversed) flow values have been carefully identified and confirmed using three techniques. They are as follows; velocity predictions using commercially available CFD software ANSYS15.0 (not shown here), the axial velocity profile drawn from hot-wire measured velocity data which are oscillating in nature, finally, the axial velocity profile measured using eight-hole Pitot static tube. The experimental axial velocity profile of Clausen *et al.* [9] is showed in fig. 8. It is confirmed that the variation in flow pattern is very less.

The velocity distribution of the swirl flow clearly indicates that the near-wall region is energized by the centrifugal force from the swirl velocity components which delayed the boundary layer separation. Another noticeable feature is that the increasing flow in the near-wall region resulted in a reduction of flow in the core region. This phenomenon has been observed by Okhio *et al.* [8] by their work on swirling flow in wide angle diffusers.

Tangential velocity

Figure 9 shows the tangential velocity distribution in 14° and 20° cone angle diffusers, respectively. The tangential velocity is normalized with the axial velocity at reference station [9]. It can be observed that, compared to the 14° diffuser, the peak swirl level decreases rapidly and shows the nearly flat distribution in the exit section of the 20° diffuser. This confirms that the swirl decay strongly depends on the cone angle and the area ratio of the diffuser.

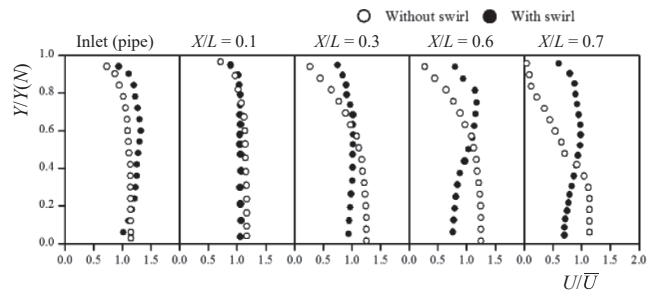


Figure 7. Axial velocity distributions in 14° diffuser

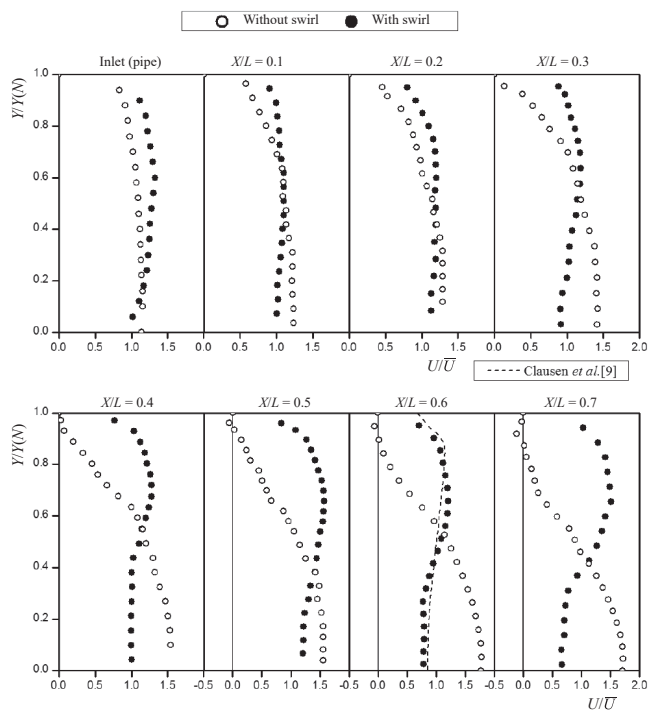


Figure 8. Axial velocity distributions in 20° diffuser

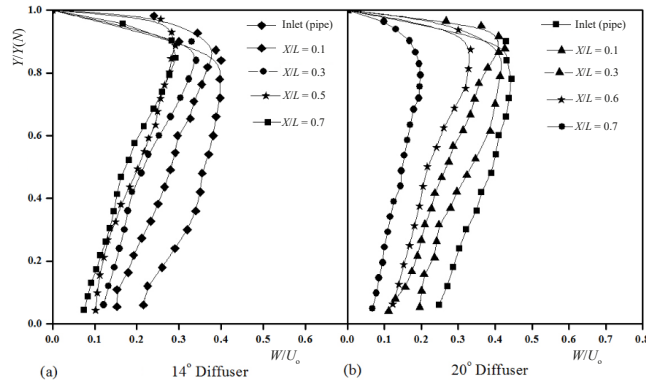


Figure 9. Tangential velocity distribution in 14° diffuser and 20° diffuser (with swirl)

Boundary layer characteristics

In order to optimize the diffuser performance and hence avoid flow separation, calculation of boundary layer characteristics is necessary. The well-defined boundary layer characteristics are displacement thickness, δ^* , the momentum thickness, θ , and shape factor, ε . They are calculated [15, 19]:

$$\delta^* = \int_0^{R(N)} \left(1 - \frac{U}{U_m}\right) \left[\frac{r}{R(N)}\right] dr \quad (6)$$

$$\theta = \int_0^{R(N)} \left(1 - \frac{U}{U_m}\right) \left(\frac{U}{U_m}\right) \left[\frac{r}{R(N)}\right] dr \quad (7)$$

$$\varepsilon = \frac{\delta}{\theta} \quad (8)$$

where U is the local velocity at a point r from the diffuser wall, U_m – the maximum velocity in the measuring section, and $R(N)$ – the diffuser radius. The equations for δ^* and θ are solved using the trapezoidal rule method. The values of displacement thickness, δ^* , the momentum thickness, θ , and shape factor, ε , are non-dimensionalised with reference to their initial values, viz. $\delta^*(i)$, and $\theta(i)$, respectively, [20]. The variation of displacement thickness ratio, $\delta^*/\delta^*(i)$, momentum thickness ratio, $\theta/\theta(i)$, and a shape factor ratio, H , along the 14° and 20° diffuser wall are given in fig. 10.

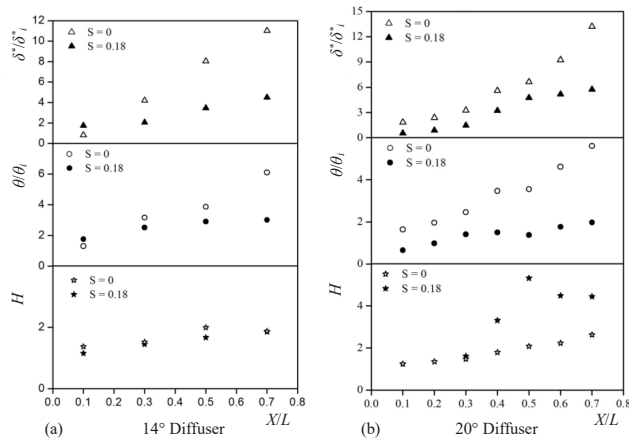


Figure 10. Variation of displacement thickness, momentum thickness and shape factor in the 14° diffuser and 20° diffuser

It is clearly seen that displacement thickness ratio, $\delta^*/\delta^*(i)$, with uniform flow increases rapidly along the length of the diffuser as the cone angle (2ϕ) increases. On the other hand, there is a marginal decrease in the displacement thickness ratio, $\delta^*/\delta^*(i)$, with the swirl in both the diffusers.

However, when the flow reaches to the exit of the diffuser section that trend is not followed; this is due to the fact that the decay of swirl is faster at higher area ratios and cone angles. It is

seen that similar trends of the displacement thickness ratio, $\delta^*/\delta^*(i)$, are followed for the momentum thickness ratio, $\theta/\theta(i)$, and a shape factor ratio, H .

Fluctuating components

The root mean square values of velocity fluctuations in radial directions are measured for the cases without swirl and with swirl. The fluctuating velocity components are normalized with the velocity, U_{ref} , at the reference station and the radial distance r is normalized with the diffuser radius, R , at each station. Figures 11 and 12 show the fluctuating components in 20° cone angle diffuser with and without swirl.

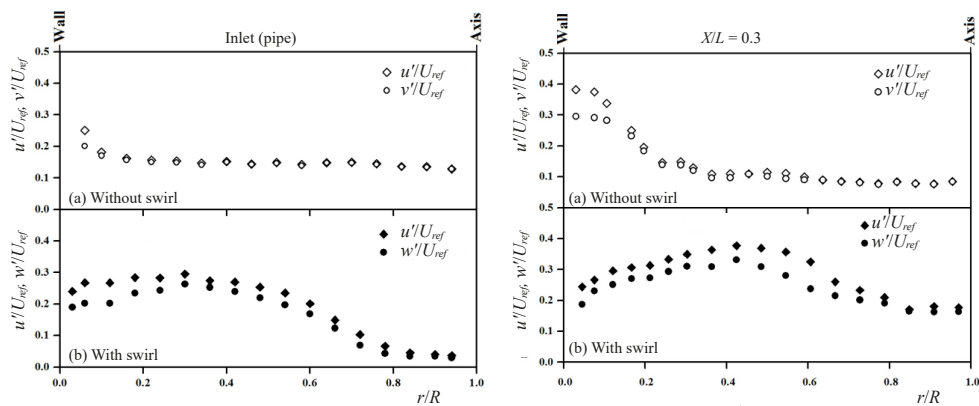


Figure 11. Distribution of fluctuating components in 20° diffuser at the reference station (inlet pipe) and $X/L = 0.3$

It is seen from the figs. 11 and 12(a) (without swirl) that the turbulent fluctuations in the uniform flow reached maximum values very close to the wall; they reached a low value in the core region. Further very close to the wall, the general relation $u' > v'$ is followed, however, near the center of the diffuser (diffuser axis) the flow tends to be isotropic ($u' \approx v'$).

Figures 11 and 12(b) (with swirl) show the distribution of u' and w' for 20° cone angle diffuser with a swirl at the inlet. In this case also, the trend $u' > w'$ is found to be valid in the boundary layer region and the flow is nearly isotropic ($u' \approx w'$) in the core region. The peak values of velocity fluctuations are found to shift away from the wall in the streamwise direction; this peak value of fluctuations clearly indicates that the effect of swirl in the turbulence intensities. The same trend has been observed in the 14° cone angle diffuser with the uniform flow and swirl type velocity distortions at the inlet (not shown here).

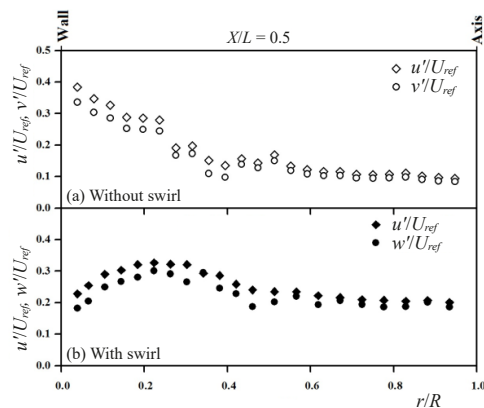


Figure 12. Distribution of fluctuating components in 20° diffuser at $X/L = 0.5$

Conclusions

The present experimental investigations of wide angle conical diffusers with uniform flow and swirl flow lead to the following conclusion.

- The introduction of a moderate swirl improves the performance of the stalled (20° cone angle diffuser) diffuser; for the diffuser (14° cone angle diffuser) having incipient turbulent boundary layer separation, the addition of moderate swirl has a little effect on the diffuser performance.
- It is clearly observed from the axial velocity profiles that flow separation is greatly controlled by the swirl flow. It may also infer from the tangential velocity profiles that the swirl decay is rapid in higher cone angle and area ratio. This confirmed that the geometrical parameter plays an important role in the diffusion process in the diffuser.
- It is confirmed that the cone angle and area ratio are the important parameter in the boundary layer development rather than the diffuser length.
- The location of the maximum turbulent fluctuations shifts away from the wall in the case of swirl flow.

Nomenclature

C_p	– pressure recovery coefficient, [–]	Y	– distance measured from the conical diffuser axis to the wall, [mm]
D	– outer diameter of annular swirl generator, [mm]	<i>Greek symbols</i>	
d	– inner diameter of annular swirl generator, [mm]	α	– hub ratio, ($= d/D$), [–]
L	– length of the conical diffuser, [mm]	β	– angle between an axis of the swirl generator to the guide vane, [°]
q	– dynamic head, ($= \rho U^2/2$), [Pa]	δ	– displacement thickness, [mm]
$R(N)$	– radius of the diffuser, [mm]	ε	– shape factor, [–]
S	– swirl number, [–]	θ	– momentum thickness, [mm]
T_0	– ambient reference temperature, [°C]	ρ	– density of air, [kgm^{-3}]
T_w	– sensor temperature, [°C]	ϕ	– half cone angle of the diffuser, [°]
U	– axial velocity, [ms^{-1}]		
X	– distance measured from the inlet along the conical diffuser axis, [mm]		

References

- [1] McDonald, A. T., Fox, R. W., An Experimental Investigation of Incompressible Flow in Conical Diffusers, *International Journal of Mechanical Sciences*, 8 (1966), 2, pp. 125IN5131-130IN6139
- [2] Okwuobi, P. A. C., Azad, R. S., Turbulence in a Conical Diffuser with Fully Developed Flow at Entry, *Journal of Fluid Mechanics*, 57 (1973), 3, pp. 603-622
- [3] Klein, A., Effects of Inlet Conditions on Conical-Diffuser Performance, *Journal of Fluids Engineering*, 103 (1981), 2, pp. 250-257
- [4] Azad, R. S., Turbulent Flow in a Conical Diffuser: A Review, *Experimental Thermal and Fluid Science*, 13 (1996), 4, pp. 318-337
- [5] Mahalakshmi, N. V., et al., Experimental Investigations of Flow through Conical Diffusers with and without Wake Type Velocity Distortions at Inlet, *Experimental Thermal and Fluid Science*, 32 (2007), 1, pp. 133-157
- [6] Van Dewoestine, R. V., et al., Effects of Swirling Inlet Flow on Pressure Recovery in Conical Diffusers, *AIAA Journal*, 9 (1971), 10, pp. 2014-2018
- [7] Senoo, Y., et al., Swirl Flow in Conical Diffusers, *Bulletin of JSME*, 21 (1978), Jan., pp. 112-119
- [8] Okhio, C. B., et al., Effects of Swirl on Flow Separation and Performance of Wide Angle Diffusers, *International Journal of Heat and Fluid Flow*, 4 (1983), 4, pp. 199-206
- [9] Clausen, P. D., et al., Measurements of a Swirling Turbulent Boundary Layer Developing in a Conical Diffuser, *Experimental Thermal and Fluid Science*, 6 (1993), 1, pp. 39-48
- [10] Lai, Y. G., et al., Calculation of Planar and Conical Diffuser Flows, *AIAA J.*, 27 (1989), 5, pp. 542-548

- [11] Jiang, G., *et al.*, Numerical Prediction of Inner Turbulent Flow in Conical Diffuser by Using a New Five-Point Scheme and DLR k - ε Turbulence Model, *Journal of Central South University of Technology*, 15 (2008), Suppl. 1, pp. 181-186
- [12] Armfield, S. W., Fletcher, C. A. J., Numerical Simulation of Swirling Flow in Diffusers, *International Journal for Numerical Methods in Fluids*, 6 (1986), 8, pp. 541-556
- [13] Chou, N. H., Fletcher, C. A. J., Computation of Turbulent Conical Diffuser Flows Using a Non-Orthogonal Grid System, *Computers & Fluids*, 19 (1991), 3-4, pp. 347-361
- [14] Okhio, C. B., *et al.*, The Calculation of Turbulent Swirling Flow through Wide Angle Conical Diffusers and the Associated Dissipative Losses, *International Journal of Heat and Fluid Flow*, 7 (1986), 1, pp. 37-48
- [15] From, C. S., *et al.*, Turbulent Dense Gas Flow Characteristics in Swirling Conical Diffuser, *Computers & Fluids*, 149 (2017), June, pp. 100-118
- [16] Jorgenson, F., *How to Measure Turbulence with Hot Wire Anemometers*, Dantec Dynamics, Skovlunde, Denmark, 2004
- [17] Bilen, K., *et al.*, Heat Transfer from a Plate Impinging Swirl Jet, *International Journal of Energy Research*, 26 (2002), 4, pp. 305-320
- [18] Lefebvre, A. H., *Gas Turbine Combustion*, CRC Press, Boca Raton, Fla., USA, 1998
- [19] Jeyachandran, K., Ganesan, V., Numerical Modelling of Turbulent Flow through Conical Diffusers with the Uniform and Wake Velocity Profiles at the Inlet, *Mathematical and Computer Modelling*, 10 (1988), 2, pp. 87-97
- [20] Ganesan, V., Flow and Boundary Layer Development in Straight Core Annular Diffusers, *International Journal of Engineering Science*, 18 (1980), 2, pp. 287-304